Flexible C–C Bonds: Reversible Expansion, Contraction, Formation, and Scission of Extremely Elongated Single Bonds

Takuya Shimajiri,[a] Takanori Suzuki,[a] and Yusuke Ishigaki*[a]

[a] T. Shimajiri, Prof. Dr. T. Suzuki, Dr. Y. Ishigaki
Department of Chemistry, Faculty of Science
Hokkaido University
Sapporo 060-0810 (Japan)
E-mail: yishigaki@sci.hokudai.ac.jp

Supporting information for this article is given via a link at the end of the document.

Abstract: Since carbon–carbon (C–C) covalent bonds are rigid and robust, the bond length is, in general, nearly constant and depends only on the bond order and hybrid orbitals. We report here direct visualization of the reversible expansion and contraction of a Csp^3–Csp^3 single bond by light and heat. This flexibility of a C–C bond was demonstrated by X-ray analyses and Raman spectroscopy of hexaphenylethane (HPE)-type hydrocarbons with two spiro-dibenzocycloheptatriene units, where intramolecular [2+2] photocyclization and thermal cleavage of the resulting cyclobutane ring both occur in a single-crystalline phase. The force constant of the contracted C–C bond is 1.6 times greater than that of the expanded bond. Since formation of the cyclobutane ring and contraction of the C–C bond lower the HOMO level by ca. 1 eV, the oxidative properties of these HPEs having a flexible C–C bond can be deactivated/activated by light/heat.

Introduction

Carbon–carbon (C–C) covalent bonds represent the most fundamental concept in organic chemistry. Elucidation of their nature is of great importance for further understanding of chemical phenomena; for instance, to understand what happens at the limits of a bond. Since deviation from the standard causes a large loss of bonding energy, structural parameters such as bond length and bond angle are nearly constant among carbon atoms. However, strained molecules such as sterically-congested polycyclic aromatic hydrocarbons[1–8] as well as cyclic π-conjugated compounds[9–15] exhibit unusual parameters, and thus have attracted much attention due to their potential applications. With regard to the C–C single bond, which has a standard length of 1.54 Å, three approaches have been taken to increase the bond length in neutral organic compounds to beyond 1.7 Å: (i) diamondoid dimers,[16] (ii) fused or clamped hexaphenylethanes (HPEs),[17–19] and (iii) diaminocarboranes (Figure 1).[20] Among these, we focused on the second approach (ii) while adopting the core-shell strategy, which enables the isolation of stable dispiro[dibenzocycloheptatriene (DBCHT)]-type HPEs **1** with an extremely elongated Csp^3–Csp^3 bond [1.806(2) Å for **1c** at 400 K]. We envisaged that such a "hyper covalent bond" should be weak enough to exhibit reversible expansion, contraction, formation, and scission, which could be visualized by X-ray analyses.

The key point is the DBCHT unit, which has been used to construct photoresponsive molecules based on overcrowded ethylenes through *syn*/*anti* isomerization.[21,22] Another aspect is a structurally fixed *cis*-stilbene moiety in the DBCHT unit, and thus the intramolecular [2+2] cycloaddition reaction could proceed as in DBCHT-dimer to produce a caged molecule.[23] The latter reactivity is more interesting from a topochemical point of view, since the solid-state reaction would be applicable for stimuli-responsive systems toward potential applications such as photoswitching, optical recording, and sensing materials.[24–32] By controlling the crystal packing structure, intermolecular [2+2] cyclization could proceed in a single-crystal-to-single-crystal (SCSC) manner upon photoirradiation, which has been realized by the aid of soft matter/lattices such as ionic crystals, metal-organic frameworks, and coordination polymers.[33–38] Furthermore, only a few examples exhibit reversible SCSC photocycloaddition and thermal cleavage of a cyclobutane ring,[34–36] and none of them are pure neutral organic molecules.

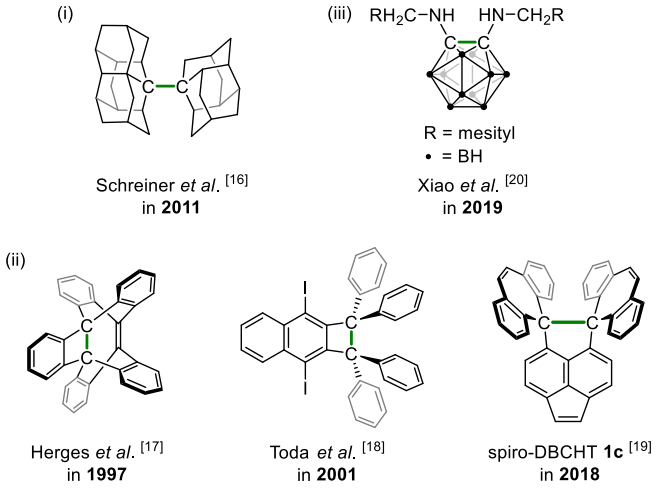

Figure 1. Previously reported molecules. Three approaches have been used to make compounds with an elongated C–C bond, which is surrounded only by (i) sp^3-hybridized carbons, (ii) sp^2-hybridized carbons, or (iii) heteroatoms.

Since *cis*-stilbene moieties connected by an elongated C–C bond face each other in the outer 'shell'-structure of

dispiro(DBCHT)-type HPEs **1a**-**1c**, we expect that a reversible SCSC [2+2] photocycloaddition and thermal cycloreversion could proceed in the pure hydrocarbon crystal. Once a [2+2] photocycloaddition reaction occurs for the spiro-DBCHT **1a**-**1c**, changes not only in physical properties but also in the bond length of the 'core' C–C bond should be observed. This paper describes how the reversible formation and scission of C–C bonds in a single crystal can be induced by external stimulation of light and heat, accompanied by reversible expansion and contraction of the elongated Csp^3–Csp^3 bond and by a change of the HOMO level by ca. 1 eV.

Results and Discussion

According to the structures of **1a**-**1c**,[19] two DBCHT units are well-overlapped due to π-π interaction with a C--C distance of 3.163(3)-3.357(4) Å between the vinylic carbons. Thus, we first photoirradiated $CHCl_3$ solutions of **1a**-**1c** at around 365 nm, which is assigned to an absorption band of DBCHT units by time-dependent density functional theory (TD-DFT) calculations (Figure S11). As a result, [2+2] photocyclization proceeded quantitatively in all spiro-DBCHT **1a**-**1c** to produce caged molecules **2a**-**2c** (Scheme 1), which was monitored by UV/Vis

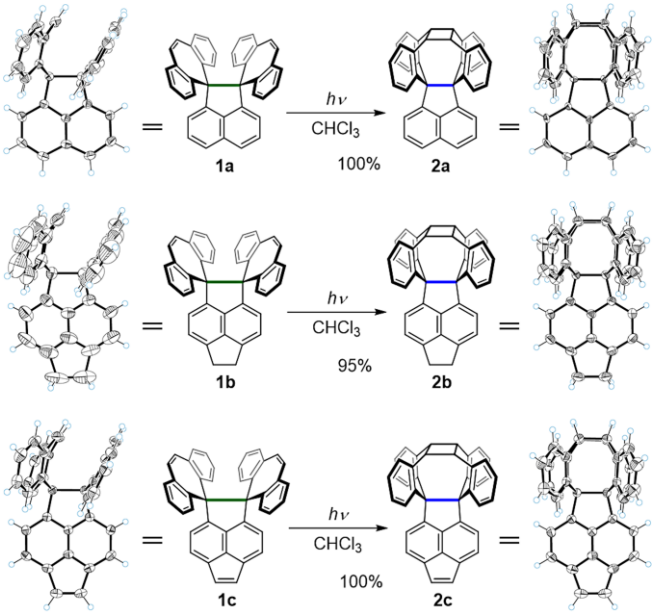

Scheme 1. Isolated yields of **2a**-**2c** upon photoirradiation with a 375 nm light-emitting diode, and ORTEP drawings at 200 K of **1a**-**1c** and **2a**-**2c**.

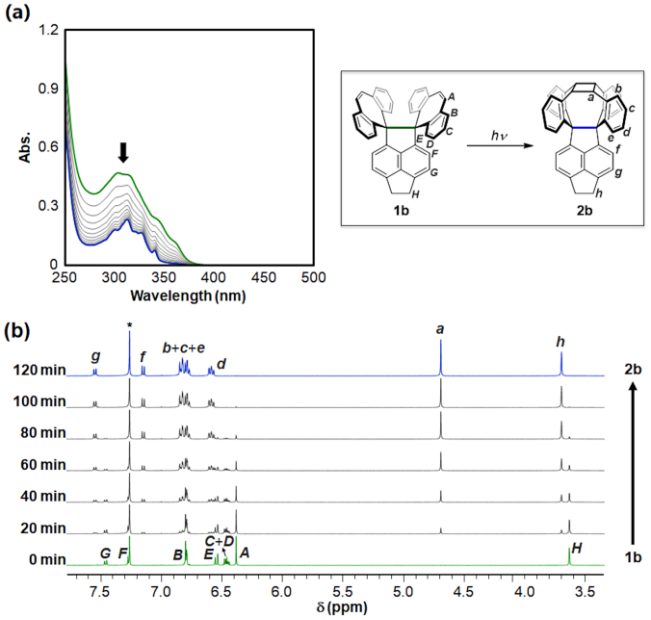

Figure 2. (a) Change in UV/Vis spectrum of **1b** (green) to **2b** (blue) in $CHCl_3$ (every 5 min) and (b) change in ^1H NMR spectrum of **1b** (green) to **2b** (blue) in $CDCl_3$ upon photoirradiation at 365 nm (Spectrofluorometer: 150 W, Xe lamp, slit width: 10 nm). The residual proton signal of the solvent ($CHCl_3$, δ = 7.26 ppm) is marked with an asterisk.

and NMR spectroscopies (Figures 2, S14, and S15). Cleavage of the cyclobutane ring in **2a**-**2c** did not occur upon photoirradiation at any wavelength. Disappearance of *cis*-stilbene moieties results not only in a blue-shift and hypochromic shift of the absorption band, but also in switching of the major chromophores to the acenaphthene ring which is located far from the cyclobutane ring. X-ray analyses revealed that **2a**-**2c** adopt caged structures with a four-membered ring (Scheme 1). A remarkable point is that contraction of the central C–C single bond by as much as ~5%, from 1.720(2)-1.742(2), 1.773(3), and 1.7980(18) Å for spiro-DBCHT **1a**, **1b**, and **1c** to 1.676(6)-1.678(6), 1.7133(16), and 1.7129(19) Å for caged molecules **2a**, **2b**, and **2c**, respectively, was observed at 200 K (Table 1). To verify the bonding nature of the contracted C–C single bond, we investigated the stretching vibration of caged molecules **2a**-**2c** by Raman spectroscopy with single crystals at 298 K to attain direct information of the bond strength. Observed Raman shifts corresponding to the central C–C bond were 653, 646, and 648 cm^{-1} for **2a**, **2b**, and **2c**, respectively, which are consistent with the simulated values (663, 653, and 658 cm^{-1}) and ~11% greater than those for **1a**-**1c** (Table 1 and Figures S16-S18). The estimated force constant (173.9 N m^{-1}) obtained as a second derivative of the energy to the bond length by DFT

Table 1. Central C–C bond lengths and Raman shifts for **1** and **2** determined by X-ray analyses (at 200 K) and Raman spectroscopy (at 298 K) with single crystals. Theoretically obtained HOMO and LUMO energy levels based on DFT calculations at the B3LYP/6-31G* level.

		1a	**2a**	**1b**	**2b**	**1c**	**2c**
C–C bond length (Å)	Expt.	1.720(2)-1.742(2)	1.676(6)-1.678(6)	1.773(3)	1.7133(16)	1.7980(18)	1.7129(19)
Raman shift (cm^{-1})	Expt.	650	653	582	646	587	648
Energy level (eV)	LUMO	–1.36	–1.06	–1.30	–0.88	–1.94	–1.94
	HOMO	–5.29	–5.58	–5.24	–5.35	–5.33	–5.77

calculations (M06-2X/6-31G*) for **2c** is 1.6 times as large as that for **1c** (108.3 N m^{-1}) (Figure S12).

Since HPEs with an elongated C–C single bond can undergo two-electron oxidation to give bond-dissociated dicationic species, as found in dynamic redox (*dyrex*) systems,[39] the redox potentials of spiro-DBCHT **1a**-**1c** and caged molecules **2a**-**2c** were measured by cyclic voltammetry in CH_2Cl_2 at ambient temperature (Figure 3a). While two-electron oxidation occurs at lower potentials for the former with an expanded bond (E^{ox}/V vs SCE: +0.93 for **1a**, +0.65 for **1b**, and +0.57 and +0.69 for **1c**), one-wave two-electron oxidation peaks appeared at much higher potentials for the latter with a contracted bond (E^{ox}/V: +1.59 for **2a**, +1.36 for **2b**, and +1.66 for **2c**) (Figures 3a,d). Especially in **1c**/**2c**, we found the largest difference in potential of about 1.1 eV before and after photocyclization. This change can be explained as follows: (i) the through-bond interaction that causes an increasing in the HOMO level would be maximized by expansion of the C–C single bond[40,41] and (ii) the coefficients in HOMO are located on the DBCHT unit and the elongated σ-bond in **1**, whereas the coefficients are located on the acenaphthene, pyracene, or dihydropyracylene skeleton in **2** based on DFT calculations (Figures S10 and S13). On the other hand, two-electron reduction peaks were found in the far cathodic region due to cleavage of the elongated C–C bond to give $\mathbf{3}^{2+}$ or $\mathbf{4}^{2+}$ (*dyrex* behavior). It should be noted that reduction peaks in the voltammograms of **1** and **2** appear at almost the same potentials, indicating that the two-electron oxidation of caged molecules **2** could induce not only scission of the central C–C bond but also cleavage of cyclobutane ring.

To gain further insight into the mechanism of three-bond scission in the oxidation of **2**, we conducted cyclic voltammetry at 195 K in CH_2Cl_2 using **2b**. As shown in Figures 3b-d, another reduction peak appeared at a less cathodic region (E^{red}/V: +0.99), which is far different from that in the reduction of $\mathbf{3b}^{2+}$ (E^{red}/V: +0.46), and thus caged dication $\mathbf{4b}^{2+}$ was generated by the oxidation of **2b** through scission of the central C–C bond even at low temperatures, whereas thermal cleavage of the cyclobutane ring of $\mathbf{4b}^{2+}$ produces bond-dissociated dication $\mathbf{3b}^{2+}$ at room temperature. Based on the voltammetric analysis, deeply colored dications $\mathbf{3a}^{2+}$-$\mathbf{3c}^{2+}$ were successfully isolated as stable $(SbCl_6^-)_2$ salts by treatment of spiro-DBCHT **1a**-**1c** with two equivalents of $(4\text{-}BrC_6H_4)_3N^{+\bullet}SbCl_6^-$ in CH_2Cl_2, due to stabilization of the dibenzotropylium units (Scheme 2 and S19). Although formation of the same dication from caged molecules **2** was demonstrated by the electrochemical oxidation of **1b**/**2b** and **1c**/**2c** (Figures S20-S23), **2a**-**2c** with lower HOMO levels need a stronger oxidant $(2,4\text{-}Br_2C_6H_3)_3N^{+\bullet}SbCl_6^-$ in CH_2Cl_2 to give the same dications $\mathbf{3a}^{2+}$-$\mathbf{3c}^{2+}$. Thus, completely selective oxidation of **1b** in a 1:1 mixture of **1b** and **2b** was achieved by using $(4\text{-}BrC_6H_4)_3N^{+\bullet}SbCl_6^-$. This means that spiro-DBCHT **1** can be protected against oxidation by conversion into caged molecules **2** with a lower HOMO level.

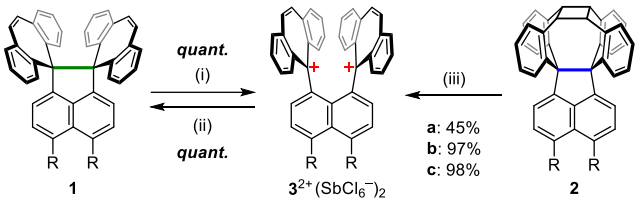

Scheme 2. Redox interconversion among **1**, **2**, and $\mathbf{3}^{2+}(SbCl_6^-)_2$. (i) $(4\text{-}BrC_6H_4)_3N^{+\bullet}SbCl_6^-$ (2.0 eq)/CH_2Cl_2. (ii) Zn (excess)/CH_3CN or THF. (iii) $(2,4\text{-}Br_2C_6H_3)_3N^{+\bullet}SbCl_6^-$ (2.0 eq)/ CH_2Cl_2. [**a** (R = H); **b** (R,R = CH_2-CH_2); **c** (R,R = CH=CH)]

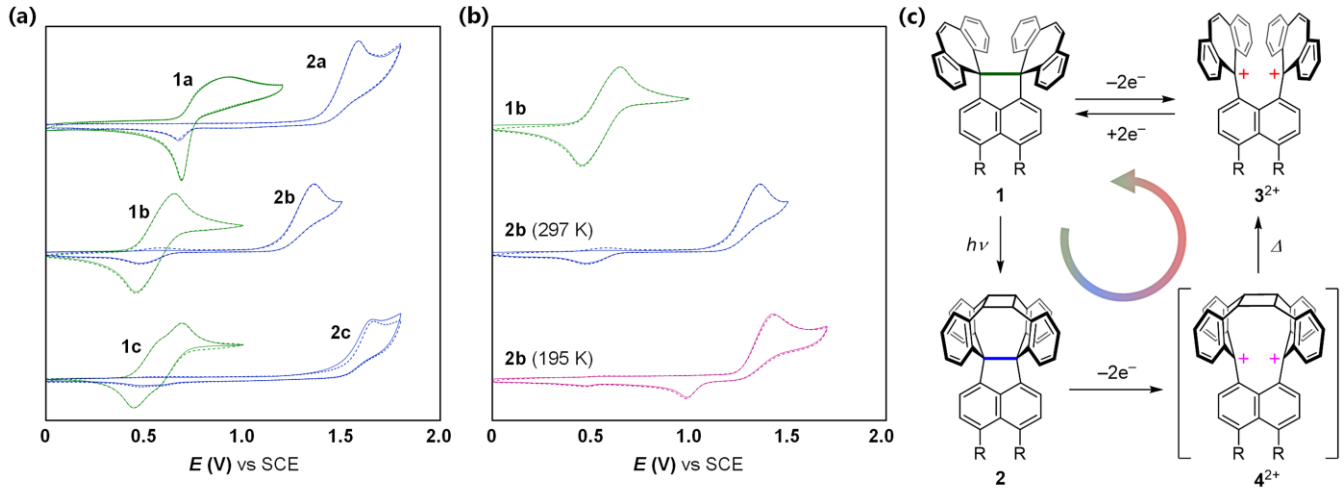

(d)

	1a	2a	1b	2b		1c	2c
T (K)	297		297		195	297	
E^{ox} (V)	+0.93 (2e)	+1.59 (2e)	+0.65 (2e)	+1.36 (2e)	+1.43 (2e)	+0.57, +0.69	+1.66 (2e)
	$\mathbf{3a}^{2+}$	$\mathbf{3a}^{2+}$	$\mathbf{3b}^{2+}$	$\mathbf{3b}^{2+}$	$\mathbf{4b}^{2+}$	$\mathbf{3c}^{2+}$	$\mathbf{3c}^{2+}$
E^{red} (V)	+0.69 (2e)	+0.67 (2e)	+0.46 (2e)	+0.47 (2e)	+0.99 (2e)	+0.58, +0.44	+0.59, +0.48

Figure 3. Cyclic voltammograms of (a) **1** and **2** at 297 K and (b) **1b**, **2b** (at 297 K), and **2b** (at 195 K) in CH_2Cl_2 containing 0.1 M Bu_4NBF_4 as a supporting electrolyte (scan rate 0.1 V s^{-1}, Pt electrode). The second cycles are shown by a dotted line. (c) Mechanism of redox interconversion. (d) Redox potentials are summarized and peak potentials are shown as E^{ox} and E^{red}. [**a** (R = H); **b** (R,R = CH_2-CH_2); **c** (R,R = CH=CH)]

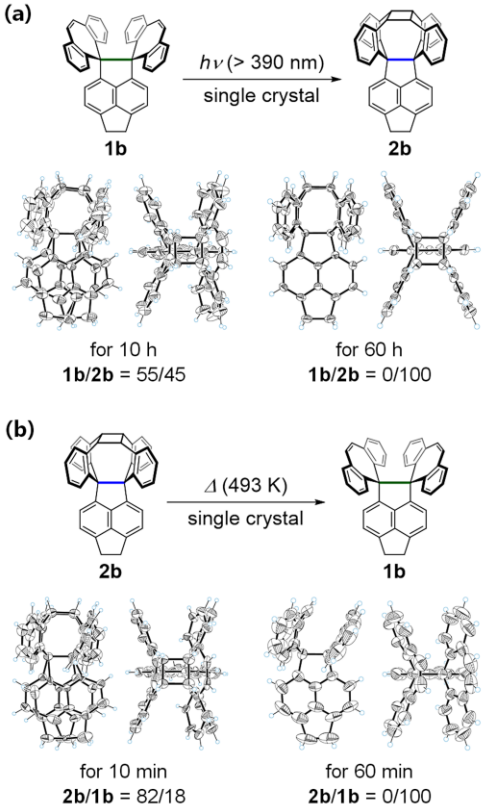

(c)

measured at 200 K	**1b**	**1b/2b**	**1b/2b**	**2b**
Photoirradiation	-	10 h	60 h	-
Ratio	100	55/45	0/100	100
***a* (Å)**	12.782(2)	12.9352(3)	13.26411(14)	13.25273(12)
***b* (Å)**	9.228(2)	9.05991(18)	8.78016(8)	8.78403(9)
***c* (Å)**	24.084(4)	23.7724(4)	23.6884(2)	23.6979(2)
***β* (°)**	100.159(3)	98.6273(16)	97.1720(9)	97.1488(8)
***V* (Å³)**	2796.2(8)	2754.41(9)	2737.19(5)	2737.28(4)
C–C bond length (Å)	1.773(3)	1.738(3)	1.7118(15)	1.7133(16)
R1	0.0633	0.0672	0.0411	0.0422
wR2	0.1968	0.1883	0.1099	0.1147

(d)

measured at 300 K	**2b**	**2b/1b**	**2b/1b**	**1b**
Heating	-	10 min	60 min	-
Ratio	100	82/18	0/100	100
***a* (Å)**	13.26469(12)	13.1312(2)	12.8016(3)	12.79971(16)
***b* (Å)**	8.83221(9)	8.93972(15)	9.2206(3)	9.22089(12)
***c* (Å)**	23.79279(19)	23.8993(4)	24.0574(7)	24.0558(3)
***β* (°)**	97.2129(8)	97.3675(17)	99.953(3)	100.0421(11)
***V* (Å³)**	2765.42(4)	2782.36(8)	2796.97(13)	2795.68(6)
C–C bond length (Å)	1.7135(16)	1.724(2)	1.777(3)	1.772(3)
R1	0.0423	0.0559	0.0751	0.0879
wR2	0.1223	0.1727	0.2329	0.2601

Figure 4. (a) Upon photoirradiation of a single crystal of **1b** with λ > 390 nm for 10 h and 60 h, the SCSC photocycloaddition reaction proceeded in respective yields of 45% and 100%, which were determined by a single-crystal X-ray analysis at 200 K. (b) When a single crystal of **2b** was heated at 493 K for 10 min and 60 min, SCSC thermal cycloreversion proceeded in respective yields of 18% and 100%, which were determined by a single-crystal X-ray analysis at 300 K. Thermal ellipsoids are shown at the 30% probability level for intermediates and the 50% probability level for completely converted samples. (c,d) The crystallographic data for **1b** and **2b** are summarized in the table.

By considering the similarity of the crystal packing and lattice parameters of **1b** and **2b**, we envisaged that both the photocyclization of **1b** and the thermal cycloreversion of **2b** would proceed in a single-crystalline state. When a single crystal of **1b** was photoirradiated at its absorption end so that the light can be penetrated into the deep inside of the crystal (λ > 390 nm) for 10 h, caged molecule **2b** was generated with maintaining single-crystallinity, and the proportion of **2b** was as high as 45% as determined by a single-crystal X-ray analysis at 200 K. This transformation is accompanied by contraction of the central C–C bond from 1.773(3) Å to 1.738(3) Å (Figures 4a,c). After photoirradiation of **1b** for 60 h, conversion to **2b** was completed while maintaining single-crystallinity, where the contracted bond length [1.7118(15) Å] is essentially the same as that [1.7133(16) Å] in the recrystallized sample of **2b**. In addition, upon heating of a single crystal of **2b** at 493 K for 10 min, thermal cleavage of the cyclobutane ring proceeded in 18% yield, and thermal isomerization proceeded completely after heating for 60 min, which was followed by single-crystal X-ray diffraction at 300 K (Figures 4b,d). As a result of the ring-opening of cyclobutane, the central C–C bond was certainly expanded to the original value [1.777(3) Å], which is in good agreement with that [1.772(3) Å] in the recrystallized sample of **1b**, thanks to the outstanding stability of the long-bonded compound **1b** at high temperature. These results show that reversible SCSC transformation occurred between **1b** and **2b**, accompanied by unprecedented expansion and contraction of the elongated C–C bond. Although single-crystallinity was not maintained for the pairs **1a/2a** and **1c/2c**, quantitative [2+2] photocyclization and thermal cleavage of the cyclobutane ring were also achieved in the solid state (Figure S24).

We then could demonstrate that both spiro-DBCHT **1** and caged molecules **2** react with an oxidant to produce dication $\mathbf{3}^{2+}$ in a solid state. When **1b** was subjected to grinding with two equivalents of blue-colored $(4\text{-}BrC_6H_4)_3N^{+\bullet}SbCl_6^-$, the color changed to deep purple with the formation of dicationic dye $\mathbf{3b}^{2+}$, which was confirmed by the appearance of characteristic IR absorptions assigned to $\mathbf{3b}^{2+}(SbCl_6^-)_2$ (*e.g.* 1601 and 1385 cm^{-1}) and the resulting amine (*e.g.* 1486 and 1311 cm^{-1}) (Figures 5a,d). Moreover, grinding of **2b** with two equivalents of green-colored $(2,4\text{-}Br_2C_6H_3)_3N^{+\bullet}SbCl_6^-$ smoothly led to the formation of a deep purple powder of dication salt $\mathbf{3b}^{2+}(SbCl_6^-)_2$, where three-bond scission proceeded in a solid state (Figures 5b,e). Additionally, upon grinding of $\mathbf{3b}^{2+}(SbCl_6^-)_2$ with an excess amount of Zn powder, $\mathbf{3b}^{2+}$ underwent two-electron reduction to give long-bonded **1b** (Figures 5c,f). This is the first example of flexible C–C bond exhibiting the reversible expansion, contraction, formation, and scission of a Csp^3–Csp^3 single bond in a simple organic compound, especially in a pure hydrocarbon.

Conclusion

We have demonstrated that photo- and thermal isomerization between spiro-DBCHT **1** and caged molecules **2** proceeded quantitatively in a solid state, where the reversible formation and

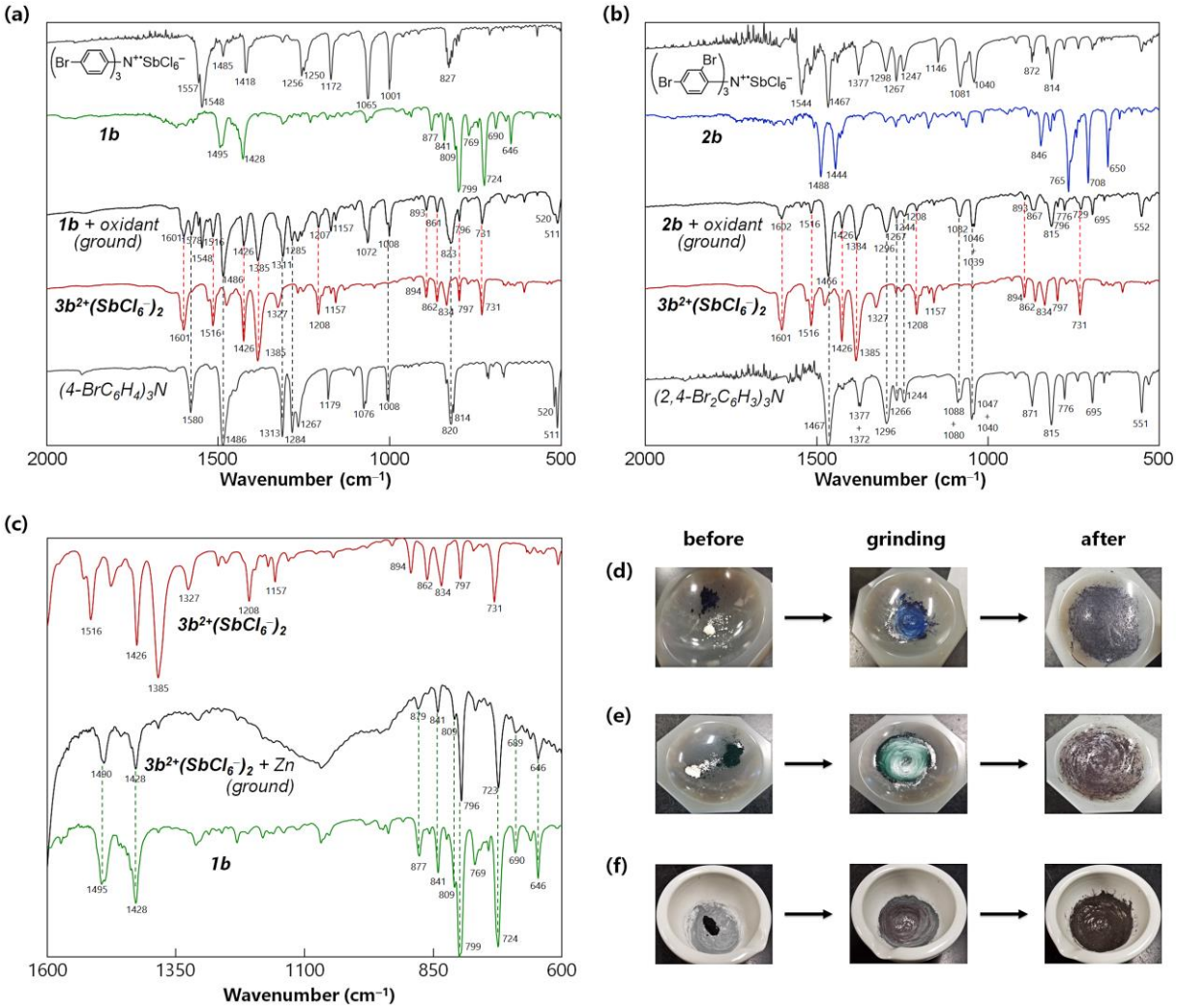

Figure 5. (a) Solid-state oxidation of **1b** with two equivalents of $(4\text{-}BrC_6H_4)_3N^{+\bullet}SbCl_6^-$ was confirmed by IR spectroscopy. (b) Solid-state oxidation of **2b** with two equivalents of $(2,4\text{-}Br_2C_6H_3)_3N^{+\bullet}SbCl_6^-$ as a stronger oxidant was confirmed by IR spectroscopy. (c) Solid-state reduction of $\mathbf{3b}^{2+}(SbCl_6^-)_2$ with an excess amount of Zn powder was confirmed by IR spectroscopy. Photographs of mechano-oxidation of (d) **1b** with $(4\text{-}BrC_6H_4)_3N^{+\bullet}SbCl_6^-$ and (e) **2b** with $(2,4\text{-}Br_2C_6H_3)_3N^{+\bullet}SbCl_6^-$, and (f) mechano-reduction of $\mathbf{3b}^{2+}(SbCl_6^-)_2$ with an excess amount of Zn powder.

scission of two C–C bonds were accompanied by expansion and contraction of the central C–C bond. Since formation of the cyclobutane ring and contraction of the C–C bond induce lowering of the HOMO level, oxidative properties can be deactivated/activated by light/heat. Caged molecules **2** generated by the photoirradiation of spiro-DBCHT **1** undergo two-electron oxidation to transiently produce bond-dissociated dications $\mathbf{4}^{2+}$ followed by thermal cleavage of the cyclobutane ring to give stable dications $\mathbf{3}^{2+}$. An elongated C–C bond was reformed by two-electron reduction of dications $\mathbf{3}^{2+}$, resulting in the formation of original spiro-DBCHT **1**. Notably, all of these processes can proceed in a solid state. This paper provides a new perspective on C–C bonds that exhibit reversible expansion, contraction, formation, and scission. Thus hydrocarbons that contain a 'flexible' C–C bond could be promising candidates for the development of functional materials, whose crystals, films, or polymers can respond to the external stimuli such as light and heat with anisotropic expansion and contraction of the matter as well as reversible switching of oxidative properties.

Acknowledgements

This work was supported by JSPS KAKENHI Grant Numbers JP19K15528, JP20H02719, and JP20K21184, and JSPS Grant-in-Aid for Research Fellow JP19J20831. Y.I. acknowledges Toyota Riken Scholar and The NOVARTIS Foundation (Japan) for the Promotion of Science. T.Sh. is grateful for the Ministry of Education, Culture, Sports, Science and Technology through the Program for Leading Graduate Schools (Hokkaido University "Ambitious Leader's Program").

Keywords: long bond • single-crystalline reaction • cyclization • thermal cycloreversion • redox chemistry

[1] M. A. Majewski, M. Stępień, *Angew. Chem. Int. Ed.* **2019**, *58*, 86–116; *Angew. Chem.* **2019**, *131*, 90–122.

[2] M. Saito, H. Shinokubo, H. Sakurai, *Mater. Chem. Front.* **2018**, *2*, 635–661.

[3] S. H. Pun, Q. Miao, *Acc. Chem. Res.* **2018**, *51*, 1630–1642.

[4] T. Hosokawa, Y. Takahashi, T. Matsushima, S. Watanabe, S. Kikkawa, I. Azumaya, A. Tsurusaki, K. Kamikawa, *J. Am. Chem. Soc.* **2017**, *139*, 18512–18521.

[5] Q. Wang, P. Hu, T. Tanaka, T. Y. Gopalakrishna, T. S. Herng, H. Phan, W. Zeng, J. Ding, A. Osuka, C. Chi, J. Siegel, J. Wu, *Chem. Sci.* **2018**, *9*, 5100–5105.

[6] Y. Nakakuki, T. Hirose, K. Matsuda, *J. Am. Chem. Soc.* **2018**, *140*, 15461–15469.

[7] Y. Xiao, J. T. Mague, R. H. Schmehl, F. M. Haque, R. A. Pascal, *Angew. Chem. Int. Ed.* **2019**, *58*, 2831–2833; *Angew. Chem.* **2019**, *131*, 2857–2859.

[8] Y. Hu, G. M. Paternò, X.-Y. Wang, X.-C. Wang, M. Guizzardi, Q. Chen, D. Schollmeyer, X.-Y. Cao, G. Cerullo, F. Scotognella, K. Müllen, A. Narita, *J. Am. Chem. Soc.* **2019**, *141*, 12797–12803.

[9] G. Povie, Y. Segawa, T. Nishihara, Y. Miyauchi, K. Itami, *Science* **2017**, *356*, 172–175.

[10] K. Y. Cheung, S. Gui, C. Deng, H. Liang, Z. Xia, Z. Liu, L. Chi, Q. Miao, *Chem* **2019**, *5*, 838–847.

[11] Y. Segawa, M. Kuwayama, Y. Hijikata, M. Fushimi, T. Nishihara, J. Pirillo, J. Shirasaki, N. Kubota, K. Itami, *Science* **2019**, *365*, 272–276.

[12] Y. Ni, T. Y. Gopalakrishna, H. Phan, T. Kim, T. S. Herng, Y. Han, T. Tao, J. Ding, D. Kim, J. Wu, *Nat. Chem.* **2020**, *12*, 242–248.

[13] M. Rickhaus, M. Jirasek, L. Tejerina, H. Gotfredsen, M. D. Peeks, R. Haver, H.-W. Jiang, T. D. W. Claridge, H. L. Anderson, *Nat. Chem.* **2020**, *12*, 236–241.

[14] T. Mio, K. Ikemoto, S. Sato, H. Isobe, *Angew. Chem. Int. Ed.* **2020**, *59*, 6567–6571; *Angew. Chem. Int. Ed.* **2020**, *132*, 6629–6633.

[15] T. A. Schaub, E. A. Prantl, J. Kohn, M. Bursch, C. R. Marshall, E. J. Leonhardt, T. C. Lovell, L. N. Zakharov, C. K. Brozek, S. R. Waldvogel, S. Grimme, R. Jasti, *J. Am. Chem. Soc.* **2020**, *142*, 8763–8775.

[16] P. R. Schreiner, L. V Chernish, P. A. Gunchenko, E. Y. Tikhonchuk, H. Hausmann, M. Serafin, S. Schlecht, J. E. P. Dahl, R. M. K. Carlson, A. A. Fokin, *Nature* **2011**, *477*, 308–311.

[17] S. Kammermeier, P. G. Jones, R. Herges, *Angew. Chem. Int. Ed. Engl.* **1997**, *36*, 1757–1760; *Angew. Chem.* **1997**, *109*, 1825–1828.

[18] K. Tanaka, N. Takamoto, Y. Tezuka, M. Kato, F. Toda, *Tetrahedron* **2001**, *57*, 3761–3767.

[19] Y. Ishigaki, T. Shimajiri, T. Takeda, R. Katoono, T. Suzuki, *Chem* **2018**, *4*, 795–806.

[20] J. Li, R. Pang, Z. Li, G. Lai, X.-Q. Xiao, T. Müller, *Angew. Chem. Int. Ed.* **2019**, *58*, 1397–1401; *Angew. Chem.* **2019**, *131*, 1411–1415.

[21] J. Luo, K. Song, F. long Gu, Q. Miao, *Chem. Sci.* **2011**, *2*, 2029–2034.

[22] Y. Ishigaki, Y. Hayashi, T. Suzuki, *J. Am. Chem. Soc.* **2019**, *141*, 18293–18300.

[23] M. Pillekamp, W. Alachraf, I. M. Oppel, G. Dyker, *J. Org. Chem.* **2009**, *74*, 8355–8358.

[24] B. L. Feringa, *J. Org. Chem.* **2007**, *72*, 6635–6652.

[25] M. Irie, T. Fukaminato, K. Matsuda, S. Kobatake, *Chem. Rev.* **2014**, *114*, 12174–12277.

[26] V. García-López, D. Liu, J. M. Tour, *Chem. Rev.* **2020**, *120*, 79–124.

[27] M. Baroncini, S. Silvi, A. Credi, *Chem. Rev.* **2020**, *120*, 200–268.

[28] P. Ravat, T. Šolomek, D. Häussinger, O. Blacque, M. Juríček, *J. Am. Chem. Soc.* **2018**, *140*, 10839–10847.

[29] C. L. Fleming, S. Li, M. Grøtli, J. Andréasson, *J. Am. Chem. Soc.* **2018**, *140*, 14069–14072.

[30] T. Yang, Y. Wang, X. Liu, G. Li, W. Che, D. Zhu, Z. Su, M. R. Bryce, *Chem. Commun.* **2019**, *55*, 14582–14585.

[31] P. Lentes, E. Stadler, F. Röhricht, A. Brahms, J. Gröbner, F. D. Sönnichsen, G. Gescheidt, R. Herges, *J. Am. Chem. Soc.* **2019**, *141*, 13592–13600.

[32] N.-Y. Li, J.-M. Chen, X.-Y. Tang, G.-P. Zhang, D. Liu, *Chem. Commun.* **2020**, *56*, 1984–1987.

[33] K. Novak, V. Enkelmann, G. Wegner, K. B. Wagener, *Angew. Chem. Int. Ed. Engl.* **1993**, *32*, 1614–1616; *Angew. Chem.* **1993**, *105*, 1678–1680.

[34] G. K. Kole, T. Kojima, M. Kawano, J. J. Vittal, *Angew. Chem. Int. Ed.* **2014**, *53*, 2143–2146; *Angew. Chem. Int. Ed.* **2014**, *126*, 2175–2178.

[35] N.-Y. Li, D. Liu, B. F. Abrahams, J.-P. Lang, *Chem. Commun.* **2018**, *54*, 5831–5834.

[36] G. Pahari, B. Bhattacharya, C. M. Reddy, D. Ghoshal, *Chem. Commun.* **2019**, *55*, 12515–12518.

[37] I. E. Claassens, L. J. Barbour, D. A. Haynes, *J. Am. Chem. Soc.* **2019**, *141*, 11425–11429.

[38] J. Zhang, J. Li, X. Feng, M. Kong, Z. Hu, Y.-X. Zheng, Y. Song, *Chem. Commun.* **2019**, *55*, 12873–12876.

[39] T. Suzuki, H. Tamaoki, J. Nishida, H. Higuchi, T. Iwai, Y. Ishigaki, K. Hanada, R. Katoono, H. Kawai, K. Fujiwara, T. Fukushima, in *Organic Redox Systems: Synthesis, Properties and Applications, Chapter 2,* Wiley, **2015**, 13–37.

[40] R. Hoffmann, *Acc. Chem. Res.* **1971**, *4*, 1–9.

[41] Y. Ishigaki, Y. Hayashi, K. Sugawara, T. Shimajiri, W. Nojo, R. Katoono, T. Suzuki, *Molecules* **2017**, *22*, 1900.

Entry for the Table of Contents

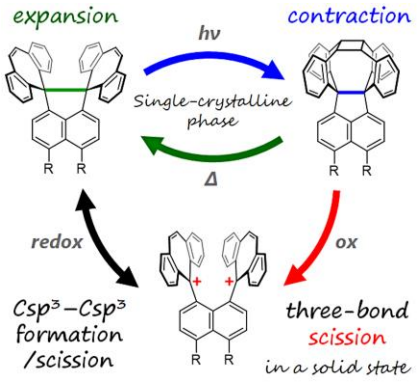

Flexible C–C bond! Reversible expansion and contraction of a Csp^3–Csp^3 single bond triggered by light/heat were certainly visualized by single crystal X-ray analyses. In combination with redox chemistry, reversible interconversion was demonstrated between long bonded neutral species and stable dication, accompanied by C–C bond formation and scission. All processes can proceed in a solid state.

Institute and researcher Twitter usernames: Twitter usernames: lab (@Yuuichi_Hokudai) and Yusuke Ishigaki (@ysk_isgk)